

Geometric Fabrics for the Acceleration-based Design of Robotic Motion

Mandy Xie^{*1,2}, Karl Van Wyk^{*1}, Anqi Li^{1,3}, Muhammad Asif Rana^{1,2},
Qian Wan¹, Dieter Fox^{1,3}, Byron Boots^{1,3}, and Nathan Ratliff¹

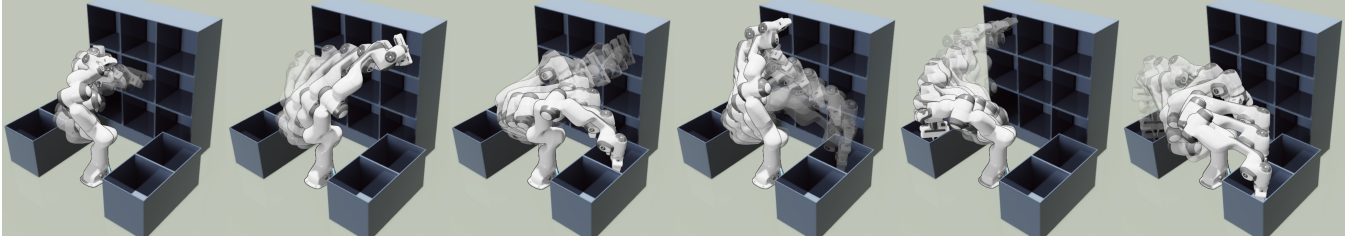


Fig. 1. Robot seamlessly navigating cubbies using a geometric fabric that enables obstacle and joint limit avoidance, redundancy resolution, and end-effector reaching. Videos available at <https://sites.google.com/nvidia.com/geometric-fabrics>.

Abstract—This paper describes the pragmatic design and construction of geometric fabrics for shaping a robot’s task-independent nominal behavior, capturing behavioral components such as obstacle avoidance, joint limit avoidance, redundancy resolution, global navigation heuristics, etc. Geometric fabrics constitute the most concrete incarnation of a new mathematical formulation for reactive behavior called optimization fabrics. Fabrics generalize recent work on Riemannian Motion Policies (RMPs); they add provable stability guarantees and improve design consistency while promoting the intuitive acceleration-based principles of modular design that make RMPs successful. We describe a suite of mathematical modeling tools that practitioners can employ in practice and demonstrate both how to mitigate system complexity by constructing behaviors layer-wise and how to employ these tools to design robust, strongly-generalizing, policies that solve practical problems one would expect to find in industry applications. Our system exhibits intelligent global navigation behaviors expressed entirely as fabrics with zero planning or state machine governance.

I. INTRODUCTION

Fast, reactive motion is essential for most modern tasks, especially in highly-dynamic and uncertain collaborative environments. We describe here a set of tools built from *geometric fabrics*, derived from our recent theory of *optimization fabrics* [1], for the direct construction of *stable* robotic behavior in modular parts.¹ Fabrics define a nominal behavior independent of a specific task, capturing cross-task commonalities like joint-limit avoidance, obstacle avoidance, and redundancy resolution, and implement a task as an optimization problem across the fabric. The fabric defines behavior by shaping the optimization path. Geometric fabrics specifically characterize behavior as generalized nonlinear geometries. We derive tools for designing these fabrics and demonstrate their utility on a Franka Panda robot in a standard setting commonplace in industry.

^{*}Equal contribution, ¹All authors are with (or interned at) NVIDIA, ²Georgia Tech, ³University of Washington

¹The term *fabric* is used analogously to the term *fabric of spacetime* from theoretical physics, but formalizes the idea as a second-order nonlinear differential equation characterizing an *unbiased* nominal behavior.

A. Related work

In [2] the authors observed that even systems built on classical planning [3] or optimization [4, 5, 6] require a layer of real-time reactive control leveraging techniques like operational space control [7] when addressing collaborative problems. Research into Riemannian Motion Policies (RMPs) [8, 9] built on these observations and proposed a behavioral design framework, embedding more globally aware behaviors into reactive control, powerful enough to develop strongly-generalizing systems² often circumventing standard planning architectures entirely.

Optimization fabrics [1] are the culmination of that line of work into a comprehensive mathematical theory of behavioral design with rigorous stability guarantees, and geometric fabrics are their concrete incarnation. Earlier systems orchestrated RMPs in system applications using complex state machines to skirt the difficulty of designing nonlinear policies directly. These limitations motivated work on learning highly nonlinear RMPs from demonstration [10, 11, 12], but it proved challenging to integrate policy learning with existing RMP systems.

A theoretical result discussed in [1] (Section I.A) shows that a fundamental limitation of many techniques, such as operational space control [7, 13], geometric control [14], and geometric dynamical systems [9], which we now understand as Lagrangian fabrics within the theory of fabrics, is that all of those systems *either* have fundamentally limited expressivity *or* they must express behavior through objective potentials (excludes velocity dependence) which creates conflicting objectives. This observation suggests that the challenges of incorporating learned RMPs stemmed from using the subclass of classical mechanical systems (a form of Lagrangian fabric). This paper studies the broader class of *geometric fabric* which is provably more flexible, exhibits geometrical consistency (speed-independence), and inherits rigorous stability guarantees from the theory of fabrics.

²Strongly-generalizing system are systems designed and tested on a collection of validation examples that then perform robustly on an entire distribution of problems.

Future work includes revisiting learning in this context to leverage the more flexible inductive bias.

II. PRELIMINARIES

Geometric fabrics build on the theory of spectral semi-sprays (specs), detailed in our companion theoretical paper [1], which generalize the idea of modular second-order differential equations first derived and used as Riemannian Motion Policies (RMPs) in [8, 9]. Let \mathcal{C} be the d -dimensional configuration space of the robot. Throughout this paper, we will use vector-notation describing elements of a space in coordinates. Mapped task spaces $\mathbf{x} = \phi(\mathbf{q})$ are defined in coordinates³ denoting $\mathbf{q} \in \mathcal{C} \subset \mathbb{R}^d$ and $\mathbf{x} \in \mathcal{X} \subset \mathbb{R}^n$ with Jacobian matrix $\mathbf{J} = \partial_{\mathbf{x}}\phi$, used in the relations $\dot{\mathbf{x}} = \mathbf{J}\dot{\mathbf{q}}$ and $\ddot{\mathbf{x}} = \mathbf{J}\ddot{\mathbf{q}} + \dot{\mathbf{J}}\dot{\mathbf{q}}$.

The spec algebra enables the design of differential equations in parts using transform trees [9, 1]. The tree implicitly represents a complete differential equation at the root as a sum of the parts. *Natural-form* specs $(\mathbf{M}, \mathbf{f})_{\mathcal{X}}$ represent equations of the form $\mathbf{M}(\mathbf{x}, \dot{\mathbf{x}})\ddot{\mathbf{x}} + \mathbf{f}(\mathbf{x}, \dot{\mathbf{x}}) = \mathbf{0}$, and their algebra derives from how these equations sum and transform under $\ddot{\mathbf{x}} = \mathbf{J}\ddot{\mathbf{q}} + \dot{\mathbf{J}}\dot{\mathbf{q}}$ (see [1]). *Canonical-form* specs $(\mathbf{M}, \mathbf{h})_{\mathcal{X}}^{\mathcal{C}}$ express standard acceleration-form equation $\ddot{\mathbf{x}} + \mathbf{h}(\mathbf{x}, \dot{\mathbf{x}}) = \mathbf{0}$ where $\mathbf{h} = \mathbf{M}^{-1}\ddot{\mathbf{x}}$. For robotics applications we find it useful to additionally introduce a *policy-form* spec $[\mathbf{M}, \pi]_{\mathcal{X}}$ to denote the *solved* policy expression $\ddot{\mathbf{x}} = -\mathbf{h}(\mathbf{x}, \dot{\mathbf{x}}) = \pi(\mathbf{x}, \dot{\mathbf{x}})$ to emphasize $\pi = -\mathbf{h}$ is an *acceleration policy*.

III. THEORETICAL GEOMETRIC TOOLS

The theory of generalized nonlinear geometry and Finsler energy is important for the derivation of geometric fabrics given in [1]. We give just a brief overview of key facts here sufficient for applications of geometric fabrics (see [16] for more details.)

A. Generalized nonlinear geometries

A generalized nonlinear geometry is an acceleration policy $\ddot{\mathbf{x}} = \pi(\mathbf{x}, \dot{\mathbf{x}})$ for which π has a special homogeneity property. We require that it be *positively homogeneous of degree 2* (HD2), which means that for any $\lambda \geq 0$ we have $\pi(\mathbf{x}, \lambda\dot{\mathbf{x}}) = \lambda^2\pi(\mathbf{x}, \dot{\mathbf{x}})$. One can show that the HD2 property ensures the differential equation is more than just a collection of trajectories (its integral curves); it additionally has a *path consistency* property whereby every integral curve starting from a given position \mathbf{x}_0 with velocity $\dot{\mathbf{x}}_0 = \eta\hat{\mathbf{n}}$ pointing in a given direction $\hat{\mathbf{n}}$ (here $\eta > 0$) will follow *the same path* [16]. In particular, any variant of the differential equation of the form $\ddot{\mathbf{x}} = \pi(\mathbf{x}, \dot{\mathbf{x}}) + \alpha(t, \mathbf{x}, \dot{\mathbf{x}})\dot{\mathbf{x}}$, where $\alpha \in \mathbb{R}$, will have integral curves that trace out the same paths as π . That geometric consistency property turns π into a *geometry of paths*.

³The spec algebra defines covariant transforms, so the behavior is independent of curvilinear changes of coordinates [15]. For notational simplicity, we express our results a single choice of coordinates.

B. Finsler energies

A Finsler energy $\mathcal{L}_e(\mathbf{x}, \dot{\mathbf{x}})$ is a generalization of classical kinetic energy from classical mechanics (the classical kinetic energy $\mathcal{K} = \frac{1}{2}\dot{\mathbf{x}}^T \mathbf{G}(\mathbf{x})\dot{\mathbf{x}}$ is a form of Finsler energy). Analogous to the classical case, the Euler-Lagrange equation applied to a Finsler energy defines an equation of motion $\mathbf{M}_e(\mathbf{x}, \dot{\mathbf{x}})\ddot{\mathbf{x}} + \mathbf{f}_e(\mathbf{x}, \dot{\mathbf{x}}) = \mathbf{0}$ where $\mathbf{M}_e = \partial_{\dot{\mathbf{x}}\dot{\mathbf{x}}}\mathcal{L}_e$ is the *energy (or metric) tensor* and $\mathbf{f}_e = \partial_{\dot{\mathbf{x}}\mathbf{x}}\mathcal{L}_e\dot{\mathbf{x}} - \partial_{\mathbf{x}}\mathcal{L}_e$ captures curvature terms (Coriolis and centripetal forces in classical mechanics). This equation matches the classical mechanical equations of motion when $\mathcal{L}_e = \mathcal{K}$, for which $\mathbf{M}_e(\mathbf{x}, \dot{\mathbf{x}}) = \mathbf{G}(\mathbf{x})$.

In geometric fabrics, the energy tensor defines the policy's *priority metric* and the curvature terms \mathbf{f}_e are used for stability (see Section VI-C). Finsler energies are Lagrangians, $\mathcal{L}_e(\mathbf{x}, \dot{\mathbf{x}})$, that satisfy

- 1) Positivity: $\mathcal{L}_e(\mathbf{x}, \dot{\mathbf{x}}) \geq 0$ with equality only for $\dot{\mathbf{x}} = \mathbf{0}$.
- 2) Homogeneity: $\mathcal{L}_e(\mathbf{x}, \dot{\mathbf{x}})$ is positively homogenous of degree 2 in $\dot{\mathbf{x}}$; i.e. for $\lambda \geq 0$ we have $\mathcal{L}_e(\mathbf{x}, \lambda\dot{\mathbf{x}}) = \lambda^2\mathcal{L}_e(\mathbf{x}, \dot{\mathbf{x}})$.
- 3) Energy tensor invertibility: $\mathbf{M}_e = \partial_{\dot{\mathbf{x}}\dot{\mathbf{x}}}\mathcal{L}_e$ is everywhere invertible.

The metric tensor $\mathbf{M}_e(\mathbf{x}, \dot{\mathbf{x}})$ is in general a function of *velocity* as well as position, although the above homogeneity requirement enforces that \mathbf{M}_e depends only on the *directionality* of the velocity ($\mathbf{M}_e(\mathbf{x}, \dot{\mathbf{x}}) = \mathbf{M}_e(\mathbf{x}, \hat{\mathbf{x}})$ for $\dot{\mathbf{x}} \neq \mathbf{0}$) and not the magnitude (i.e. it is homogeneous of degree 0). This dependence on directionality enables us to design directionally dependent priority matrices in Section VI as metric tensors of Finsler energies.

IV. GEOMETRIC FABRICS

Geometric fabrics are a form of *optimization fabric* [1] which is a special type of differential equation designed to induce *behavior* by influencing the optimization path of a differential optimizer.⁴ Here we describe pragmatically how to effectively design the fabric to encode a desired behavior.

A *forced geometric fabric* is a collection of *fabric terms* defined as pairs $(\mathcal{L}_e, \pi)_{\mathcal{X}}$ of a Finsler energy $\mathcal{L}_e(\mathbf{x}, \dot{\mathbf{x}})$ and an acceleration policy $\ddot{\mathbf{x}} = \pi(\mathbf{x}, \dot{\mathbf{x}})$. Geometric terms define the fabric while forcing terms define the objective. A *geometric term* is a term $(\mathcal{L}_e, \pi_2)_{\mathcal{X}}$ for which π_2 is an HD2 geometry. A *forcing term* is a term $(\mathcal{L}_e, -\mathbf{M}_e^{-1}\partial_{\mathbf{x}}\psi)_{\mathcal{X}}$ which derives its policy from a potential function. Fabric terms can be added to spaces of a transform tree [9] for the modular design of composite behaviors.

Each fabric term defines a triple $(\mathbf{M}_e, \mathbf{f}_e, \pi)_{\mathcal{X}}$, where $\mathbf{M}_e\ddot{\mathbf{x}} + \mathbf{f}_e = \mathbf{0}$ derives from the Euler-Lagrange equation applied to \mathcal{L}_e [16], which can be viewed as two specs, a policy spec $[\mathbf{M}_e, \pi]_{\mathcal{X}}$ and a natural energy spec $(\mathbf{M}_e, \mathbf{f}_e)_{\mathcal{X}}$. Geometric fabric summation and pullback is, accordingly, defined in terms of the algebra of these two constituent specs.

Geometric fabrics are *unbiased* and thereby never prevent a system from reaching a local minimum of the objective.

⁴The *optimization path* is the system trajectory generated when a fabric is forced by the negative gradient of an objective.

The objective, therefore, encodes concrete task goals independent of the fabric’s behavior. Additionally, geometric policies are geometrically consistent speed-invariant geometry of paths, which both simplifies the intuition on how they sum and enables behavior-invariant execution speed control.

The design of a geometric fabric follows the intuition of designing RMPs [8]. Policy specs $[\mathbf{M}_e, \pi_2]_{\mathcal{X}}$ model both a desired behavior π_2 and a priority matrix on that behavior \mathbf{M}_e defining how it combines with other policies as a metric-weighted average of parts. The spectrum of \mathbf{M}_e can assign different weights to different directions in the space, and both $\pi_2(\mathbf{x}, \dot{\mathbf{x}})$ and $\mathbf{M}_e(\mathbf{x}, \dot{\mathbf{x}})$ have the flexibility of depending on both position \mathbf{x} and velocity $\dot{\mathbf{x}}$. Since \mathbf{M}_e is HD0 (see Section III-B), geometric terms remain geometric under summation and pullback (e.g. the policy resulting from a metric-weighted average of geometries is itself a geometry). The energy spec $(\mathbf{M}_e, \mathbf{f}_e)_{\mathcal{X}}$ of each fabric term is used only to guarantee stability during execution (see Section V). Practitioners can, therefore, simply focus on designing the behavior policy specs $[\mathbf{M}_e, \pi_2]_{\mathcal{X}}$.

V. EXECUTION AND ALGORITHMS

Once the forced geometric fabric is designed, one can transform it by accelerating and decelerating along the direction of motion using the methodology outlined in [1] (see also Section VI-C) to maintain a given measured of *execution energy* (e.g. speed of the end-effector or joint speed through the configuration space). The geometric consistency of the fabric ensures the behavior remains consistent despite these speed modulations. Many numerical integrators are appropriate for integrating the final differential equation. We find Euler (1ms time step) or fourth order Runge-Kutta (10ms time step) exhibit a good trade-off between speed and accuracy.

In full, we design a system in three parts (using a transform tree [9] of task spaces): (1) design the underlying behavioral fabric, (2) add a driving potential to define task goals, (3) design an execution energy for speed control.

Design of a forced geometric fabric:

- (1) Construct a transform tree.
- (2) Populate its nodes with fabric terms. Most terms are geometric terms and just a few are forcing terms (often only one).
- (3) Add execution energy specs to the tree as needed to describe the execution energy we want to control.

Execution of the forced fabric with speed control:

- (1) Forward pass: Populate the nodes with the current state from the root to the leaves.
- (2) Backward pass: Evaluate the specs and pull them to root in separate channels, an *energy channel* for the geometric terms’ energy specs, a *policy channel* for the geometric terms’ policy specs, an *execution energy channel* for the execution energy specs, and a *forcing policy channel* for the forcing terms’ policy specs. Add the forcing term’s energy specs to the energy channel.
- (3) Use the four channels’ root results to calculate the final desired acceleration using speed control.

VI. CONCRETE DESIGN TOOLS

Geometric fabrics follow acceleration-based design principles captured in the original canonical-form RMPs [8]. As described in Section IV, a geometric fabric is a pair $(\mathcal{L}_e, \pi_2)_{\mathcal{X}}$ characterizing two specs, an energy spec and a geometry spec. The energy spec captures stability information, while the geometry spec captures behavior. Behavioral design focuses on constructing the latter, using the class of HD2 geometries to model π_2 and deriving \mathbf{M}_e as the energy tensor of a Finsler geometry \mathcal{L}_e .

When geometric fabrics are summed $\sum_i (\mathcal{L}_e^{(i)}, \pi_2^{(i)})_{\mathcal{X}}$, the combined fabric’s geometry spec (capturing its behavior) $\sum_i (\mathbf{M}_e^{(i)}, \pi_2^{(i)})_{\mathcal{X}} = (\widetilde{\mathbf{M}}_e, \widetilde{\pi}_2)$ is a metric-weighted average of the contributing geometries $\widetilde{\pi}_2 = (\sum_i \mathbf{M}_e^{(i)})^{-1} \sum_i \mathbf{M}_e^{(i)} \pi_2^{(i)}$, prioritized by the total metric $\widetilde{\mathbf{M}}_e = \sum_i \mathbf{M}_e^{(i)}$. When populating a transform tree, this intuitive combination rule is applied recursively at each node. Designers need only focus on intuitively creating modular acceleration policies (as HD2 geometries) in the different spaces and prioritizing them with metric tensors (from Finsler energies).

A. Construction of HD2 Geometries

An HD2 geometry is a differential equation $\ddot{\mathbf{x}} + \mathbf{h}_2(\mathbf{x}, \dot{\mathbf{x}}) = \mathbf{0}$ where \mathbf{h}_2 is HD2 (see Section III-A), which we usually denote in *policy* form $\ddot{\mathbf{x}} = -\mathbf{h}_2(\mathbf{x}, \dot{\mathbf{x}}) = \pi_2(\mathbf{x}, \dot{\mathbf{x}})$. Constructing an HD2 geometry is straightforward given the following rules of homogeneous functions: (1) a sum of HD2 functions is HD2; (2) multiplying homogeneous functions adds their degrees (denoting an HD k function as f_k , examples are $f_2 f_0 = f_2$, $f_1 f_1 = f_2$, etc.). For instance, a simple way to design an HD2 geometry is to choose an HD0 policy $\pi_0(\mathbf{x})$ that depends only on position and form $\pi_2(\mathbf{x}, \dot{\mathbf{x}}) = \|\dot{\mathbf{x}}\|^2 \pi_0(\mathbf{x})$ by scaling it by $\|\dot{\mathbf{x}}\|^2$. $\pi_0(\mathbf{x})$ can be chosen as the negative gradient of a potential $\pi_0(\mathbf{x}) = -\partial_{\mathbf{x}} \psi(\mathbf{x})$.

B. Acceleration-based Potentials

It is often most intuitive to design a geometric fabrics’ forcing potential as a forcing *spec* $\mathcal{F} = [\mathbf{M}_f, \pi_f]_{\mathcal{X}}$ in *policy form* so it’s treated intuitively as another acceleration policy averaged into the final metric weighted average. This policy π_f must, therefore, implicitly express a *forcing potential* $\psi_f(\mathbf{x})$ whose negative gradient is given by $-\partial_{\mathbf{x}} \psi_f(\mathbf{x}) = \mathbf{M}_f \pi_f$. When designing \mathcal{F} we must enforce that \mathbf{M}_f and π_f remain theoretically compatible in that sense. Following Appendix D.4 in [17], we advocate choosing $\pi_f = -\nabla_{\mathbf{x}} \psi_{\text{acc}}(\mathbf{x})$ where ψ_{acc} is a potential function that is spherically symmetric around its global minimum expressing the acceleration policy directly as its negative gradient. Any metric $\mathbf{M}_f(\mathbf{x})$ is theoretically compatible if it is also spherically symmetric around the same global minimum point. Note that position-only metrics are Riemannian and derive from Finsler energies of the form $\mathcal{L}_e = \frac{1}{2} \dot{\mathbf{x}}^T \mathbf{M}_f(\mathbf{x}) \dot{\mathbf{x}}$.

C. Speed control

We follow the speed control methodology outlined in [1]. Specifically, that entails using $\alpha_{\text{reg}} = \alpha_{\text{ex}}^n - \beta_{\text{reg}}(\mathbf{x}, \dot{\mathbf{x}}) +$

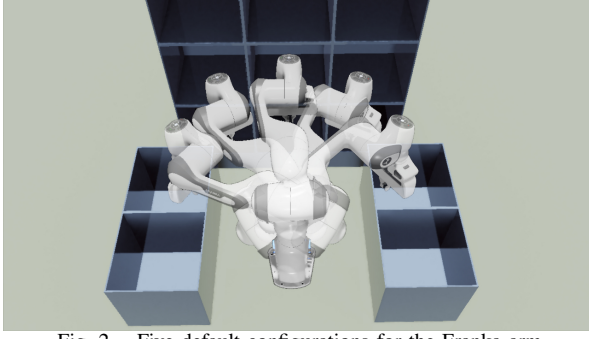


Fig. 2. Five default configurations for the Franka arm.

α_{boost} in $\ddot{\mathbf{x}} = -\mathbf{M}_e^{-1}\partial_{\mathbf{x}}\psi(x) + \pi_0(\mathbf{x}, \dot{\mathbf{x}}) + \alpha_{\text{reg}}\dot{\mathbf{x}}$ with $\beta_{\text{reg}} = s_{\beta}(\mathbf{x})B + \underline{B} + \max\{0, \alpha_{\text{ex}}^{\eta} - \alpha_{\mathcal{L}_e}\}$ (see [1] for details). $\underline{B} > 0$ is a (small) baseline damping, the $B > \underline{B}$ is a larger damping coefficient for succinct convergence. The switch $s_{\beta}(\mathbf{x})$ turns on close to the target:

$$s_{\beta}(\mathbf{x}) = \frac{1}{2} \left(\tanh(-\alpha_{\beta}(\|\mathbf{x}\| - r)) + 1 \right) \quad (1)$$

where $\alpha_{\beta} \in \mathbb{R}^+$ is a gain defining the switching rate, and $r \in \mathbb{R}^+$ is the radius where the switch is half-way engaged. Denoting the desired execution energy as $\mathcal{L}_e^{\text{ex,d}}$, we use the following policy for η

$$\eta = \frac{1}{2} \left(\tanh(-\alpha_{\eta}(\mathcal{L}_e^{\text{ex}} - \mathcal{L}_e^{\text{ex,d}}) - \alpha_{\text{shift}}) + 1 \right) \quad (2)$$

where $\alpha_{\eta}, \alpha_{\text{shift}} \in \mathbb{R}^+$ adjust the rate and offset, respectively, of the switch as an affine function of the speed (execution energy) error. Finally, α_{boost} is modeled as $\alpha_{\text{boost}} = k\eta(1 - s_{\beta}(\mathbf{x})) \frac{1}{\|\dot{\mathbf{x}}\| + \epsilon}$, where $k \in \mathbb{R}^+$ is a gain that directly sets the desired level of acceleration, η (from above) sets $\alpha_{\text{boost}} = 0$ when the desired speed is achieved, and $1 - s_{\beta}(\mathbf{x})$ sets $\alpha_{\text{boost}} = 0$ when the system is within the region of higher damping. The normalization by $\|\dot{\mathbf{x}}\| + \epsilon$ ensures that α_{boost} is directly applied along $\hat{\mathbf{x}}$ with a very small positive value for ϵ to ensure numerical stability. This overall design injects more energy into the system when $-\alpha_{\text{boost}} < \alpha_{\text{ex}}^{\eta} - \alpha_{\mathcal{L}_e}$. Since this injection occurs for finite time, the total system energy is still bounded. The additional switches ensure that the system is still subject to positive damping, guaranteeing convergence.

VII. FRANKA ARM EXPERIMENTS

These experiments represent a global end-effector navigation problem common in many logistics, collaborative, and industrial settings, wherein a robot must autonomously interact with cubbies (bins). We demonstrate the effectiveness of the layer-wise construction of a geometric fabric (other example usage in [1] and [16]) that enables the robot to reach into and out of three sets of cubbies (see Fig. 1). There are six reachable cubbies in front and two on either side of the Franka arm. The length, width, and depth of each cubby are 0.3 m. The following discusses the fabric layers, where every new layer rests upon the previous, fixed layers, mitigating design and tuning complexity.

A. Behavioral Layers

Each policy is defined as an HD2 geometry of the form $\ddot{\mathbf{x}} = -\|\dot{\mathbf{x}}\|^2\partial_{\mathbf{x}}\psi(\mathbf{x})$. Policies are weighted by $\mathbf{M}_e(\mathbf{x}, \dot{\mathbf{x}})$ from the Finsler energy, $\mathcal{L}_e = \dot{\mathbf{x}}^T \mathbf{G}(\mathbf{x}, \dot{\mathbf{x}})\dot{\mathbf{x}}$. $\psi(\mathbf{x})$ and $\mathbf{G}(\mathbf{x}, \dot{\mathbf{x}})$ are defined as follows.

1) *Layer 1*: The first layer creates a baseline geometric fabric designed for *global*, cross-body, point-to-point end-effector navigation absent obstacles.

End-effector Attraction: Attraction towards a target uses the task map, $\mathbf{y} = \phi_{\text{att}}(\mathbf{x}) = \mathbf{x}_t - \mathbf{x}$, where $\mathbf{x}, \mathbf{x}_t \in \mathbb{R}^3$ are the current and target end-effector position in Euclidean space. The metric is simply an identity matrix scaled by $s(\|\mathbf{y}\|)$, $G_{\text{att}} = s(\|\mathbf{y}\|)\mathbf{I}$, where $s(\|\mathbf{y}\|) = 40$ if $\|\mathbf{y}\| < 0.5$, and $s(\|\mathbf{y}\|) = 1$, otherwise. The acceleration-based potential gradient, $\partial_{\mathbf{q}}\psi(\mathbf{y}) = \mathbf{M}_{\text{att}}(\mathbf{y})\partial_{\mathbf{q}}\psi_1(\mathbf{y})$, uses

$$\psi_1(\mathbf{y}) = k \left(\|\mathbf{y}\| + \frac{1}{\alpha_{\psi}} \log \left(1 + e^{-2\alpha_{\psi}\|\mathbf{y}\|} \right) \right) \quad (3)$$

where $k \in \mathbb{R}^+$ controls the overall gradient strength, $\alpha_{\psi} \in \mathbb{R}^+$ controls the transition rate of $\psi_1(\mathbf{y})$ from a positive constant to 0, and here, $\alpha_{\psi} = 10$, $k = 10$.

Joint Limit Avoidance: This behavior uses two 1D task maps per joint, $x_j^u = \phi_u(q_j) = \bar{q}_j - q_j$ and $x_j^l = \phi_l(q_j) = q_j - \underline{q}_j$, where \bar{q}_j and \underline{q}_j are the upper and lower limits of the j^{th} joint. Denoting both generically as x , the metric G_l is defined as $G_l(x, \dot{x}) = s(\dot{x})\frac{\lambda}{x}$, where $s(\dot{x}) = 0$ if $\dot{x} \geq 0$ and $s(\dot{x}) = 1$ otherwise (1D normalization), and $\lambda = 10$. Effectively, this removes the effect of the coordinate limit geometry once motion is orthogonal or away from the limit. The acceleration-based potential gradient, $\partial_q\psi_l(x) = M_l(x)\partial_q\psi_{1,l}(x)$, uses

$$\psi_{1,l}(x) = \frac{\alpha_1}{x^2} + \alpha_2 \log \left(e^{-\alpha_3(x - \alpha_4)} + 1 \right), \quad (4)$$

and $M_l(\mathbf{x})$ comes from Finsler energy $L_e(x) = G_l(x)\dot{x}^2$, where $G_l(x)$ is $G_l(x, \dot{x})$ that drops $s(\dot{x})$ term, $\alpha_1, \alpha_2 \in \mathbb{R}^+$ control the significance and mutual balance of the first and second terms. $\alpha_3 \in \mathbb{R}^+$ controls the sharpness of the smooth rectified linear unit (SmoothReLU) while $\alpha_4 \in \mathbb{R}^+$ offsets the SmoothReLU. Overall, $\psi_l(x) \rightarrow \infty$ as $x \rightarrow 0$ and $\psi_l(x) \rightarrow 0$ as $x \rightarrow \infty$, which impedes motion towards a limit. In this experiment, $\alpha_1 = 0.4$, $\alpha_2 = 0.05$, $\alpha_3 = 20$, and $\alpha_4 = \pi/6$.

Default Configuration: The task map for this behavior is $\mathbf{x} = \phi_{dc}(\mathbf{q}) = \mathbf{q}_0 - \mathbf{q}$, where \mathbf{q}_0 is a default configuration. The metric \mathbf{G}_{dc} is simply an identity matrix scaled by a constant λ_{dc} , $\mathbf{G}_{dc} = \lambda_{dc}\mathbf{I}$, where $\lambda_{dc} = 0.5$. The acceleration-based potential gradient is defined in the same way as Eq. 3, where $\alpha_{\psi} = 6.75$ and $k = 100$. Five separate default configurations are created to cover different regions of the robot (see Fig 2). This behavior controls robot posture and resolves manipulator redundancy.

2) *Layer 2*: This layer enables the end-effector to extract and enter any cubby (ignoring collision).

Cubby Extraction: Cubby extraction uses two task maps that are the distance between: 1) the end-effector and the *front plane* of the cubby, $y_1 = \phi_1(\mathbf{x}) = -\|\mathbf{x}_f - \mathbf{x}\|$ if

the end-effector is inside of the cubby, $y_1 = \phi_1(\mathbf{x}) = \|\mathbf{x}_f - \mathbf{x}\|$, otherwise, where $\mathbf{x}, \mathbf{x}_f \in \mathbb{R}^3$ are the end-effector position and its orthogonal projection onto the front plane, respectively; and 2) the end-effector and a line that is centered and orthogonal to the front plane of the target cubby, $y_2 = \phi_2(\mathbf{x}) = \|\mathbf{x}_c - \mathbf{x}\|$, where $\mathbf{x}, \mathbf{x}_c \in \mathbb{R}^3$ are the end-effector position, and the closest point on the line to the end-effector, where the line is orthogonal and centered with the front plane. The priority metric is designed as

$$G_w(\mathbf{x}) = s(y_1) \left((\bar{m} - \underline{m}) s(y_2) + \underline{m} \right) \mathbf{I}. \quad (5)$$

where $s(y_1) = 1$ if $y_1 < 0.1$ and $s(y_1) = 0$, otherwise. $s(y_2) = 0.5(\tanh(\alpha_m(y_2 - r)) + 1)$, $\bar{m}, \underline{m} \in \mathbb{R}^+$ are the upper and lower isotropic masses, respectively, and $\alpha_m \in \mathbb{R}^+$ defines the rate of transition between 0 and 1, while $r \in \mathbb{R}^+$ offsets the transition. For this experiment, $\bar{m} = 5$, $\underline{m} = 0$, $\alpha_m = 100$, and $r = 0.15$. Overall, the priority vanishes if the end-effector is either more than $0.1 m$ away from the front plane (outside of the cubby) or within $0.15 m$ of the target cubby center line. The potential function is the same as defined in Eq. 4, where $\alpha_1 = 0$, $\alpha_2 = 15$, $\alpha_3 = 100$, $\alpha_4 = 0.05$.

Target Cubby Attraction: An additional target attraction policy is used to help pull the end-effector inside a target cubby. It is the same as the end-effector attraction defined in Layer 1, but with the priority metric defined as Eq. 5, where $s(y_1) = 1 \forall y_1$, $\bar{m} = 5$, $\underline{m} = 0$, $\alpha_m = -100$, and $r = 0.15$, and $\alpha_\psi = 10$, $k = 40$ are used in Eq. 3. Overall, the priority remains zero until it enters a cylindrical region aligned with the target cubby. The heightening priority funnels motion into the cubby.

Way-Point Attraction: This term guides the arm to the cubby opening by attracting to a point $0.15m$ ahead of the front plane. The term generally matches the end-effector attraction term above, but with a different target and a switching function on the metric disabling it once within the column of the target cubby. Specifically, we make the following changes: 1) replace x_t with x_w in the task map, where $\mathbf{x}_w \in \mathbb{R}^3$ is the way point position; 2) define the switching function with the task map $y_2 = \phi_2(\mathbf{x}) = \|\mathbf{x}_c - \mathbf{x}\|$ as described in the cubby extraction policy; 3) $k = 20$ is used in Eq. 3. Note this term guides the arm but, as a geometric term, does not affect convergence to the target.

3) *Layer 3:* This layer enables complete collision avoidance with the cubbies.

Cubby Collision: The task map for this behavior is $y = \phi_c(\mathbf{x})$ which captures the minimum distance between a point on the arm and the cubby, where \mathbf{x} in \mathbb{R}^3 is a designated *collision* point on the robot. Denoting the closest point on the cubby as \mathbf{x}_c , we use $y = \phi_c(\mathbf{x}) = \|\mathbf{x}_c - \mathbf{x}\|$ (ignoring dependencies of \mathbf{x}_c on \mathbf{x} for simplicity). The metric is defined as a function of position, $G_b(y) = \frac{k_b}{y^2}$, where $k_b \in \mathbb{R}^+$ is a barrier gain. The acceleration-based potential gradient, $\partial_{\mathbf{q}} \psi_b(y) = M_b(y) \partial_{\mathbf{q}} \psi_{1,b}(y)$, uses $\psi_{1,b}(y) = \frac{\alpha_b}{y^3}$, where $\alpha_b \in \mathbb{R}^+$ is the barrier gain. Here, $k_b = 1$ and $\alpha_b = 0.1$.

B. Objective and Damping

The optimization potential is an acceleration-based design as discussed in VI-B, and it is designed for task space, $\mathbf{y} = \phi(\mathbf{x}) = \mathbf{x} - \mathbf{x}_t$, where $\mathbf{x}, \mathbf{x}_t \in \mathbb{R}^3$ are the current and target end-effector position in Euclidean space. The acceleration-based potential gradient, $\partial_{\mathbf{y}} \psi(\mathbf{y}) = M_\psi(\mathbf{y}) \partial_{\mathbf{y}} \psi_1(\mathbf{y})$, uses $\psi_1(y)$ as defined in Eq. 3 with $\alpha_\psi = 10$, $k = 20$,

$$G_\psi(\mathbf{y}) = \left((\bar{m} - \underline{m}) s(\|\mathbf{y}\|) + \underline{m} \right) \mathbf{I}, \quad (6)$$

where $s(\|\mathbf{y}\|) = 0.5(\tanh(\alpha_m(\|\mathbf{y}\| - r)) + 1)$, $\bar{m}, \underline{m} \in \mathbb{R}^+$ are the upper and lower isotropic masses, respectively, and $\alpha_m \in \mathbb{R}^+$ defines the rate of transition between 0 and 1, while $r \in \mathbb{R}^+$ offsets the transition. For this experiment, $\bar{m} = 40$, $\underline{m} = 0.1$, $\alpha_m = 100$, and $r = 0.15$. This design allows for small attraction potential when far away from the target while smoothly increasing priority as getting closer to the target location.

Damping (see VI-C) values are $B = 17.5$, $\underline{B} = 0$. In Eq. 1, $\alpha_\beta = 50$ and $r = 0.15$. In Eq. 2, $\alpha_{eta} = 10$, $\alpha_{shift} = 2$, $\mathcal{L}_e^{\text{ex}} = \mathbf{y}^T \mathbf{y}$ and $\mathcal{L}_e^{\text{ex,d}} = 1$. The gain k in α_{boost} is defined as $k = -5 \|\dot{\mathbf{y}}\| - \mathcal{L}_e^{\text{ex,d}}$, where $\|\dot{\mathbf{y}}\|$ is the current end-effector speed.

C. Results

As seen in Fig. 1, the robot intelligently navigates the cubbies. To demonstrate strong generalization, we tuned (train) the system with 6.7% (6 of 90) of the available problems (navigating between a pair of cubbies), validated it on 90 problems with a 96.7% success rate, and tested it on 90 problems with a success rate of 92.2%, where the base was rotated by 30 degrees counterclockwise. Standard tuning protocol would iterate this cycle of tuning and testing until the system performed well on the entire problem distribution; this success rate is indicative of a generally fast tuning convergence. Here, a second round of tuning easily solved the observed issues. We also tested the tuned policy on the 6 training problems with an array of perturbed variants, mimicking relocating the robot to the scene (such as with a mobile base). Perturbations to the base ($\Delta x, \Delta y, \Delta \theta$) include combinations of $(-0.1 m, \pm 0.1 m, \pm \frac{\pi}{6} rad)$ and $(-0.1 m, \pm 0.1 m, 0 rad)$. The system behaved well on all variants. We additionally verified that varying execution speed produces negligible change to paths (see supplemental videos).

VIII. CONCLUSIONS

Geometric fabrics are RMPs whose acceleration policies are HD2 geometries and whose priority metrics derive from Finsler energies. They constitute compact encoding of behavior simple enough to shape by hand. They rivals the broadest class of RMPs [8] in expressivity and add a geometric consistency enabling simple layer-wise design and speed regulation. We document concrete design tools and layering procedures effective in realistic settings. Interestingly, the strong generalization observed in our experiments suggests geometric fabrics may additionally represent a well-informed and flexible inductive bias for policy learning.

REFERENCES

- [1] N. D. Ratliff, K. V. Wyk, M. Xie, A. Li, and A. M. Rana, "Optimization fabrics for behavioral design," *arXiv:2010.15676 [cs.RO]*, 2020. [Online]. Available: <https://arxiv.org/abs/2010.15676>
- [2] D. Kappler, F. Meier, J. Issac, J. Mainprice, C. Garcia Cifuentes, M. Wüthrich, V. Berenz, S. Schaal, N. Ratliff, and J. Bohg, "Real-time perception meets reactive motion generation," *IEEE Robotics and Automation Letters*, vol. 3, no. 3, pp. 1864–1871, Jul. 2018. [Online]. Available: <https://arxiv.org/abs/1703.03512>
- [3] S. M. LaValle, *Planning Algorithms*. Cambridge, U.K.: Cambridge University Press, 2006, available at <http://planning.cs.uiuc.edu/>.
- [4] N. Ratliff, M. Toussaint, and S. Schaal, "Understanding the geometry of workspace obstacles in motion optimization," in *IEEE International Conference on Robotics and Automation (ICRA)*, 2015.
- [5] M. Mukadam, J. Dong, X. Yan, F. Dellaert, and B. Boots, "Continuous-time Gaussian process motion planning via probabilistic inference," *International Journal of Robotics Research (IJRR)*, vol. 37, no. 11, pp. 1319–1340, 2018.
- [6] T. Erez, K. Lowrey, Y. Tassa, V. Kumar, S. Koley, and E. Todorov, "An integrated system for real-time model-predictive control of humanoid robots," in *IEEE/RAS International Conference on Humanoid Robots*, 2013.
- [7] O. Khatib, "A unified approach for motion and force control of robot manipulators: The operational space formulation," *IEEE Journal of Robotics and Automation*, vol. 3, no. 1, pp. 43–53, 1987.
- [8] N. D. Ratliff, J. Issac, D. Kappler, S. Birchfield, and D. Fox, "Riemannian motion policies," *arXiv:1801.02854*, 2018.
- [9] C.-A. Cheng, M. Mukadam, J. Issac, S. Birchfield, D. Fox, B. Boots, and N. Ratliff, "RMPflow: A computational graph for automatic motion policy generation," in *The 13th International Workshop on the Algorithmic Foundations of Robotics*, 2018.
- [10] M. A. Rana, A. Li, H. Ravichandar, M. Mukadam, S. Chernova, D. Fox, B. Boots, and N. Ratliff, "Learning reactive motion policies in multiple task spaces from human demonstrations," in *Conference on Robot Learning (CoRL)*, 2019.
- [11] M. Mukadam, C.-A. Cheng, D. Fox, B. Boots, and N. Ratliff, "Riemannian motion policy fusion through learnable Lyapunov function reshaping," in *Conference on Robot Learning (CoRL)*, 2019.
- [12] A. Li, M. Mukadam, M. Egerstedt, and B. Boots, "Multi-objective policy generation for multi-robot systems using Riemannian motion policies," *CoRR*, vol. abs/1902.05177, 2019. [Online]. Available: <http://arxiv.org/abs/1902.05177>
- [13] J. Peters, M. Mistry, F. Udwadia, J. Nakanishi, and S. Schaal, "A unifying framework for robot control with redundant DOFs," *Autonomous Robots*, vol. 24, no. 1, pp. 1–12, 2008.
- [14] F. Bullo and A. D. Lewis, *Geometric control of mechanical systems: modeling, analysis, and design for simple mechanical control systems*. Springer Science & Business Media, 2004, vol. 49.
- [15] J. M. Lee, *Introduction to Smooth Manifolds*, 2nd ed. Springer, 2012.
- [16] N. D. Ratliff, K. V. Wyk, M. Xie, A. Li, and A. M. Rana, "Generalized nonlinear and Finsler geometry for robotics," *arXiv:2010.14745 [cs.RO]*, 2020. [Online]. Available: <https://arxiv.org/abs/2010.14745>
- [17] C.-A. Cheng, M. Mukadam, J. Issac, S. Birchfield, D. Fox, B. Boots, and N. Ratliff, "Rmpflow: A computational graph for automatic motion policy generation," *arXiv:1811.07049*, 2018.